Supramolecular structural influences from remote functionality in coordination complexes of 4-picolylamine ligands

V. D. Slyusarchuk, B. J. O'Brien & C. S. Hawes

View supplementary material

Published online: 12 Oct 2022.

Submit your article to this journal

Article views: 153

View related articles

View Crossmark data

Supramolecular structural influences from remote functionality in coordination complexes of 4-picolylamine ligands

V. D. Slyusarchuk, B. J. O'Brien and C. S. Hawes

School of Chemical and Physical Sciences, Keele University, Keele, UK

ABSTRACT

A series of nine cobalt(II), copper(II) and silver(I) coordination complexes of structurally similar picolylamine ligands, N-(4-picolyl)piperidine (**L1**) and N-(4-picolyl)morpholine (**L2**), have been prepared and analyzed. These consist of a dinuclear copper(II) complex $[Cu_2(OAc)_4(\textbf{L1})_2]$ (**1**), tetranuclear copper(II) complexes $[Cu_4OCl_6(\textbf{L1})_4]\cdot MeCN\cdot H_2O$ (**2**) and $[Cu_4OCl_7(\textbf{L2})_2(\textbf{L2H})]\cdot 2MeCN\cdot 9H_2O$ (**3**), trichlorocobaltate complexes $[CoCl_3(\textbf{L1H})]\cdot MeCN$ (**4**) and $[CoCl_3(\textbf{L2H})]$ (**5**), silver coordination polymers poly-$[Ag\textbf{L1}]SbF_6\cdot 0.5THF$ (**6**), poly-$[Ag(\textbf{L2})]SbF_6\cdot 0.5THF$ (**7**) and poly-$[Ag(\textbf{L1})(CO_2CF_3)]$ (**9**) and discrete dinuclear silver complex $[Ag_2(\textbf{L2})_2(THF)_4](SbF_6)_2$ (**8**). While the coordination and classical N–H···X hydrogen bonding in these species is related and largely independent of backbone functionality, differences in ligand composition dictate the d weak interactions and the supramolecular structure. In **1**, **2**, **4**, **6** and **9** piperidine acts as a weak hydrogen bond donor, with C–H···Cl/O/F contacts mostly observed from the methylene groups adjacent to the amine. In the morpholine species **3**, **5**, **7** and **8** the tendency for morpholine to associate via reciprocated C–H···O interactions overrides the other crystal packing tendencies, changing both the local and extended structures. By studying both strong and weak packing interactions, this study presents a test case for the design of discrete and polymeric coordination compounds with finely tuned modes of intermolecular interaction.

1. Introduction

The development of functional coordination materials in fields such as catalysis, sensing, and drug delivery has led to a demand for more complex materials for increasingly niche applications [1]. In order to design these materials with more targeted applications, it is imperative to gain control over the hierarchy of interactions that dictate their formation and behavior [2]. Stronger interactions such as coordination bonds are well understood and therefore relatively straightforward to design and implement as synthons in extended structures [3]. Classical hydrogen bonding or halogen bonding, while typically weaker than coordination bonding, are long-standing methods for structure direction and the association of metal complexes into higher-dimensional materials [4].

Weaker non-classical hydrogen bonding interactions involving polarized C–H donors, on the other hand, are a more challenging aspect of metallosupramolecular structure design [5]. While the energetics of the C–H···X hydrogen bond are well established as an attractive interaction [6], the comparatively small stabilization energy of such interactions places them near the level of non-directional dispersion-type interactions which govern the extended structures of weakly-interacting species [7]. While undoubtedly present as ancillary stabilizing forces in a range of crystalline coordination materials, the structural impact of these forces is easily overlooked but can have profound structural influences [8]. As such, while elegant and rationally designed coordination bonding, halogen bonding and hydrogen bonding architectures can be successfully designed *ab initio* [9], there are fewer examples of C–H hydrogen bond donors acting as intentional structural elements in coordination networks [10]. Nonetheless, the successful deployment of highly electron deficient C–H hydrogen bond donors in organic anionophores provides strong evidence as to the potential of these interactions in the design of extended structures [11].

Alkyl amines have long been an attractive class of ligands for functional coordination materials [12]. As well as their synthetic versatility, amines are important pendant functionality in porous materials due to their favorable interactions with CO_2 and other Lewis acidic guests [13]. While primary and secondary amines are commonly encountered in MOF chemistry following post-synthetic modification routes [14], ligands with tertiary alkylamine backbones have also proven important building blocks
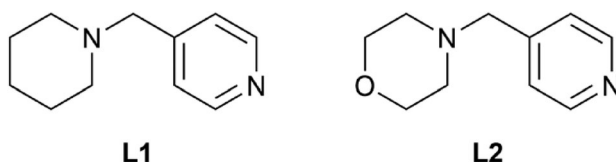
Scheme 1. Structure of N-(4-picolyl)piperidine (**L1**) and N-(4-picolyl)morpholine (**L2**).

in coordination polymers [15]. Substituted piperazines, for example, can act as semi-rigid linkers for transition metal ions either by coordination through the amine nitrogen atoms or *via* pendant coordinating groups [16]. Cyclic alkylamines may also provide a useful route into rigid non-aromatic building blocks for MOF chemistry, an emerging field in ligand design for these materials [17]. Containing only one amine group, the cyclic amines morpholine and piperidine are more commonly incorporated in functional coordination materials as electron donors for fluorophores, solubility aids or proton acceptors rather than as the basis for divergent ligands in coordination polymers [18], although both exhibit useful coordination chemistry in their own right [19]. The importance of the C–H···O contact in crystalline morpholine compared to piperidine has been noted by Parsons and coworkers [20]. Here we report the use of piperidine and morpholine-substituted 4-picolylamine ligands **L1** and **L2** (scheme 1) as simple models to probe the importance of these interactions on the extended structures of crystalline coordination compounds.

2. Experimental

2.1. Materials and methods

All starting materials, reagents and solvents, purchased from Sigma-Aldrich, TCI, Alfa Aesar or Fluorochem, were of reagent grade or better and were used as received. NMR spectroscopy was performed on a Bruker Avance III HD 400 spectrometer operating at 400 MHz for ^{1}H NMR and 101 MHz for ^{13}C NMR using deuterated solvents from Cambridge Isotope Laboratories. All spectra were referenced to the residual solvent signal and/or TMS. Elemental analysis was performed using a Thermo Flash 2000 CHNS analyzer calibrated against sulfanilamide with vanadium pentoxide as a combustion aid. Elemental analyses for **6**, **8** and **9** were carried out by the Elemental Analysis service at London Metropolitan University. Infrared spectra were recorded using a Thermo Scientific Nicolet iS10 instrument operating in ATR sampling mode. Melting points were recorded in air on a Stuart digital melting point apparatus and are uncorrected. X-ray powder diffraction patterns were measured with a Bruker D8 Advance diffractometer with Cu Kα radiation ($\lambda = 1.54178$ Å). All samples were mounted on a zero-background silicon single crystal sample holder. All samples were measured at room temperature and compared against the simulated patterns from the single crystal datasets (150 K). High resolution mass spectra were measured at the EPSRC National Mass Spectrometry Facility at Swansea University, U.K.

2.2. X-Ray crystallography

X-ray diffraction data were collected on a Bruker D8 Quest ECO diffractometer with graphite monochromated Mo Kα ($\lambda = 0.71073$ Ð) radiation. Crystals were mounted on Mitegen micromounts in NVH immersion oil, and all collections were carried out at 150 K using an Oxford cryostream. Data collections and reductions were carried out in the Bruker APEX-3 suite of programs [21], with multi-scan absorption corrections performed with SADABS [22]. All datasets were solved using intrinsic phasing methods with SHELXT and refined on F^2 with SHELXL [23, 24], within the Olex-2 GUI (ESI, Tables S1–S3) [25]. All non-hydrogen atoms were located from the Fourier difference map. Most hydrogen atoms were assigned in calculated positions with a riding model, with selected hydrogen atoms involved in hydrogen bonding interactions assigned from Fourier residuals with distance restraints when appropriate. Where lattice solvent molecules exhibited disorder, approximate occupancies were determined by free variable refinement followed by fixing these values to the nearest integer fraction where reasonable, to reduce the number of parameters in the final refinement. CCDC 2168361-2168365, 2168367-2168370. A minor (<0.05) twin was evident in **2**; no improvement to the final model was obtained by modeling this twin, but as a result a slightly larger linear weighting coefficient was used to maintain a reasonable goodness of fit. Complex **3** contains solvent channels coincident with the crystallographic 3-fold axis and no chemically sensible solvation model could be assigned to this volume without excessive constraints, and so the contribution of this volume to the measured structure factors was accounted for using the solvent masking routine in Olex-2 [26]. Hirshfeld surfaces were calculated for all compounds using CrystalExplorer version 21.5 [27], with the normalized contact surface mapping and fingerprint plots used to inform the assignment of significant directional interactions within the structures (ESI, Figures S9–S17).

2.3. Synthesis of N-(α-4-picolyl)piperidine L1

K_2CO_3 (0.500 g, 3.6 mmol), KI (20 mg, 0.12 mmol), piperidine (0.84 mL, 8.5 mmol) and 4-chloromethylpyridine hydrochloride (0.460 g, 2.80 mmol) were heated at reflux in MeCN (50 mL) for 2 h. The solution was then filtered while hot, cooled to room temperature, and concentrated *in vacuo*, giving a brown solid. This was then dissolved in water (20 mL) and brought to pH 10 using 2 M $NaOH_{(aq)}$ and the product was extracted with EtOAc (3 × 20 mL). The organic layers were combined and dried over $MgSO_4$, and the solvent was removed *in vacuo*, to give a red oil of mass 270 mg (55%). δ_H (400 MHz, $CDCl_3$) 8.52 (dd, 2H, H1, $J = 4.4$, 1.5 Hz), 7.26 (dd, 2H, H2, $J = 4.4$, 1.0 Hz), 3.46 (s, 2H, H3), 2.37 (t, 4H, H4, $J = 4.5$ Hz), 1.59 (m, 4H, H5), 1.45 (m, 2H, H6); δ_C (101 MHz, $CDCl_3$) 149.7 (C1), 148.2 (4-Py), 123.9 (C2), 62.6 (C3), 54.7 (C4), 26.0 (C5), 24.2 (C6). ν_{max}/cm^{-1} (ATR): 3385 w br, 3070 w, 3026 w, 2932s, 2852 m, 2793 m, 2758 m, 2727 w, 1930 w, 1724 w, 1639 w, 1602s, 1560 m, 1493 w, 1468 w, 1454 m, 1442 m, 1414s, 1392 w, 1370 m, 1349 m, 1319 m, 1299 m, 1278 m, 1255 w, 1220 w, 1197 w, 1154 m, 1112s, 1064 m, 1038s, 992 s, 962 w, 907 w, 863 s, 828 w, 803 s, 779 s, 728 w, 669 w, 645 w, 609 s. *m/z* (ESMS) 177.1386 ([M + H$^+$], calculated for $C_{11}H_{17}N_2$ 177.1392).

2.4. Synthesis of N-(α-4-picolyl)morpholine L2

K_2CO_3 (0.500 g, 3.6 mmol), KI (20 mg, 0.12 mmol), morpholine (0.73 mL, 9.2 mmol) and 4-chloromethylpyridine hydrochloride (0.460 g, 2.8 mmol) were heated at reflux in MeCN (50 mL) for 2 h. After this, the solution was filtered while hot, cooled to room temperature and concentrated *in vacuo*, giving an orange solid. This was dissolved in water (20 mL) and basified to pH 10 using 2 M NaOH$_{(aq)}$ and the product was extracted with EtOAc (3 × 20 mL). The organic layers were combined and dried over MgSO$_4$, and the solvent was removed *in vacuo*, to give an orange oil of mass 260 mg (53%). δ_H (400 MHz, CDCl$_3$) 8.55 (dd, 2H, H1, $J = 1.5$, 4.4 Hz), 7.29 (m, 2H, H2), 3.73 (t, 4H, H5, $J = 4.7$ Hz), 3.50 (s, 2H, H3), 2.45 (t, 4H, H4, $J = 4.4$ Hz); δ_C (101 MHz, CDCl$_3$) 149.8 (C1), 147.2 (4-Py), 123.9 (C2), 66.9 (C5), 62.1 (C3), 53.7 (C4). ν_{max}/cm^{-1} (ATR): 3365 m br, 3231 w br, 3071 w, 3029 w, 3956 m, 2914 w, 2855 m, 2810 m, 2766 w, 2685 w, 1937 w, 1731 w, 1603s, 1561 m, 1494 w, 1454 m, 1416s, 1398 w, 1371 w, 1355 m, 1321 m, 1291 m, 1270 m, 1242 w, 1223 w, 1206 w, 1112s, 1068 m, 1035 m, 1008s, 959 w, 915 m, 866 s, 812 m, 789 m, 764 w, 729 w, 629 w, 602 m. *m/z* (ESMS) 179.1179 ([M + H$^+$], calculated for C$_{10}$H$_{15}$N$_2$O 179.1184).

2.5. Synthesis of [tetrakis(μ-acetato-κO:κO′)bis{N-(α-4-picolyl-κN)piperidinyl)-copper(II)}] (complex [Cu$_2$(OAc)$_4$(L1)$_2$] 1)

L1 (11 mg, 0.063 mmol) was dissolved in MeCN (3 mL). Cu(OAc)$_2$·H$_2$O (6.0 mg, 0.030 mmol) was dissolved in MeCN (3 mL) and the two solutions were combined and left in a sealed vial. After one day, green crystals had formed and were isolated by filtration. Yield 3.4 mg (32%); m.p. 215-218 °C, ν_{max}/cm^{-1} (ATR): 2944 w, 2928 w, 2921 m, 2844 w, 2813 w, 2774 w, 2758 w, 2726 w, 2711 w, 1610s, 1618s, 1560 m, 1498 m, 1466 w, 1422s, 1397 m, 1374 m, 1371 m, 1352 m, 1333 w, 1325 w, 1298 m, 1274 w, 1267 w, 1252 w, 1222 m, 1209 w, 1198 w, 1153 m, 1122 m, 1114 m, 1109 m, 1089 w, 1065 m, 1052 w, 1040 m, 1020 m, 994 m, 985 m, 958 w, 934 w, 904 w, 890 w, 863 m, 843 m, 814 m, 807 m, 785 m, 731 w, 679 s, 627 s, 617 s; Found C, 49.75; H, 6.15; N, 8.27%; calculated for C$_{30}$H$_{44}$N$_4$O$_8$Cu$_2$, C, 50.34; H, 6.20; N, 7.87%.

2.6. Synthesis of [hexakis-μ$_2$-chlorido-μ$_4$-oxido-tetrakis(N-(α-4-picolyl-κN)piperidinyl))tetrahedro-tetracopper(II)] monoacetonitrile monohydrate (complex [Cu$_4$OCl$_6$(L1)$_4$]·MeCN·H$_2$O 2)

L1 (11 mg, 0.063 mmol) was dissolved in MeCN (3 mL). CuCl$_2$·2H$_2$O (5.0 mg, 0.029 mmol) was dissolved in MeCN (3 mL) and the two solutions were combined and left in a sealed vial. After three days, brown crystals had formed and were isolated by filtration. Yield 2.4 mg (27%); m.p. 270-272 °C (decomp.); ν_{max}/cm^{-1} (ATR): 3059 w, 2889 m, 2846 m, 2809 m, 2774 m, 2159 w, 1943 w, 1851 w, 1619s, 1557 w, 1506 m, 1470 m, 1447 w, 1434 m, 1425s, 1399 w, 1369 m, 1349 m, 1333 m, 1300 m, 1277 m, 1260 m, 1226s, 1213s, 1193 m, 1158 m, 1147 m, 1116s, 1097s, 1068s, 1035s, 997 s, 981 m, 967 m, 913 m, 853 s, 852 s, 818 s, 780 s, 733 m, 665 w, 628 s. Found C, 44.43; H, 5.40; N, 10.31%; calculated for C$_{46}$H$_{69}$N$_9$O$_2$Cl$_6$Cu$_4$ C, 44.30; H, 5.58; N, 10.11%. Single crystals for X-ray diffraction were generated by following the same procedure using methanol as the solvent instead of

acetonitrile, which gave a smaller yield of higher quality single crystals. X-ray powder diffraction confirms that the bulk material from acetonitrile is isostructural, and as such all bulk characterization was carried out on the acetonitrile solvate.

2.7. Synthesis of [hexakis-μ_2-chlorido-1:2κ^2Cl;1:3κ^2Cl;1:4κ^2Cl;2:3κ^2Cl;2:4κ^2Cl; 3:4κ^2Cl-monochlorido-4κCl-μ_4-oxido-bis(N-(α-4-picolyl-1κN:2 κN)morpholinyl))-(N-(α-4-picolyl-3κN)-NH-morpholiniumyl))-tetrahedro-tetracopper(II)] diacetonitrile nonahydrate (complex [Cu$_4$OCl$_7$(L2)$_2$(L2H)]·2MeCN·9H$_2$O 3)

L2 (11 mg, 0.062 mmol) was dissolved in MeCN (1.5 mL). CuCl$_2$·2H$_2$O (5.0 mg, 0.029 mmol) was dissolved in MeCN (1.5 mL) and the two solutions were combined. Water (20 μL) was added to the combined solution and this was left in a sealed vial. After one day, brown crystals had formed and were isolated by filtration. Yield 6.3 mg (63%); m.p. 156-159 °C (decomp.); ν_{max}/cm^{-1} (ATR): 3340 m br, 3092 w, 3058 w, 3048 w, 3026 w, 2979 w, 2963 w, 2927 w, 2863 w, 2827 w, 2584 w, 2530 m br, 2461 m, 2399 w, 2348 w, 2317 w, 2287 w, 2251 m, 1623 s, 1565 w, 1495 w, 1457 m, 1445 s, 1428 s, 1405 s, 1374 m, 1353 m, 1331 w, 1303 w, 1295 m, 1268 m, 1251 m, 1224 s, 1215 s, 1122 s, 1117 s, 1082 m, 1066 s, 1059 m, 1035 s, 1011 w, 1008 m, 974 m, 963 m, 912 m, 868 s, 825 s, 790 m, 738 m, 659 w, 627 s. The solvation for the air-dried material is variable given the disordered solvent channels; the best fit for the elemental analysis data suggests solvation of [Cu$_4$OCl$_7$(**L2**)$_2$(**L2H**)]·2MeCN·9H$_2$O; Found C, 30.95; H, 3.94; N, 8.77; calculated for C$_{34}$H$_{67}$N$_8$O$_{13}$Cl$_7$Cu$_4$ C, 31.45; H, 5.20; N, 8.63%.

2.8. Synthesis of [trichlorido-(N-(α-4-picolyl-κN)-NH-piperidiniumyl))cobalt(II)] monoacetonitrile, (complex [CoCl$_3$(L1H)]·MeCN 4)

L1 (11 mg, 0.063 mmol) was dissolved in MeCN (3 mL). CoCl$_2$·6H$_2$O (15 mg, 0.063 mmol) was dissolved in MeCN (3 mL) and the two solutions were combined and left in a sealed vial. After two days, blue crystals had formed and were isolated by filtration. Yield 5.1 mg (22%); m.p. 270-272 °C; ν_{max}/cm^{-1} (ATR): 3548 w br, 3011 m, 2956 w, 2931 w, 2781 w, 2752 w, 2249 w, 1624 s, 1464 m, 1430 s, 1368 w, 1250 w, 1227 m, 1192 w, 1153 w, 1130 w, 1107 w, 1075 m, 1063 w, 1035 s, 964 w, 954 s, 944 s, 912 w, 873 w, 853 s, 816 s, 796 w, 773 w, 666 w, 620 s; Found C, 40.53; H, 5.21; N, 10.41%; calculated for C$_{13}$H$_{20}$N$_3$Cl$_3$Co, C, 40.70; H, 5.26; N, 10.95%.

2.9. Synthesis of [trichlorido-(N-(α-4-picolyl-κN)-NH-morpholiniumyl))cobalt(II)] (complex [CoCl$_3$(L2H)] 5)

L2 (5.0 mg, 0.031 mmol) was dissolved in MeCN (3 mL). CoCl$_2$·6H$_2$O (15 mg, 0.063 mmol) was dissolved in MeCN (3 mL) and the two solutions were combined and left in a sealed vial. After three days, blue crystals had formed and were isolated by filtration. Yield 5.3 mg (47%); m.p. 162-163 °C; ν_{max}/cm^{-1} (ATR): 3449 w br, 3090 w, 3060 w, 3044 w, 2995 m, 2958 m, 2764 w, 2743 m, 2684 w, 2622 w, 1621 s, 1559 w, 1510 w, 1459 m, 1430 s, 1405 m, 1371 s, 1353 m, 1335 w, 1306 w, 1262 m, 1231 m, 1214 m, 1209 w, 1120 s, 1119 m, 1073 s, 1058 m, 1045 s, 1031 s, 1015 m, 968 s, 960 m, 909 m, 866 s,

858 s, 826 m, 822 s, 790 m, 739 w, 623 m, 609 m; Found C, 35.09; H, 4.43; N, 8.33%; calculated for $C_{10}H_{15}N_2OCl_3Co$, C, 34.86; H, 4.39; N, 8.13%.

2.10. Synthesis of catena-[μ-(N-(α-4-picolyl-1κN)piperidinyl-2κN′)silver(I) hexafluoridoantimonate(V)] hemi(tetrahydrofuran) (complex poly-[AgL1]SbF₆·0.5THF) 6

L1 (11 mg, 0.063 mmol) was dissolved in THF (2 mL). AgSbF$_6$ (18 mg, 0.052 mmol) was dissolved in THF (2 mL) and the two solutions were combined and left in a sealed vial which was wrapped in foil. After three days, colorless crystals had formed and were isolated by filtration. The crystals lose single crystallinity on extended drying in air. Yield 3.2 mg (11%); m.p. 138-141 °C (decomp.); v_{max}/cm^{-1} (ATR): 2973 w br, 2949 w, 2909 w br, 2852 m, 1618 s, 1564 m, 1503 w, 1471 m, 1451 m, 1444 m, 1433 s, 1392 w, 1373 w, 1361 m, 1343 m, 1337 w, 1304 m, 1281 m, 1251 w, 1234 m, 1186 m, 1145 w, 1113 w, 1090 m, 1082 m, 1066 s, 1059 s, 1035 s, 985 m, 971 s, 960 m, 916 m, 897 m, 891 w, 862 s, 855 s, 820 s, 803 m, 781 s, 744 w, 652 s, 644 s, 633 s. Elemental analysis suggests the lattice THF solvent molecule is lost on drying in air; Found C, 25.86; H, 3.33; N, 5.50%; calculated for $C_{22}H_{32}N_4F_{12}Sb_2Ag_2$ ([Ag$_2$(**L1**)$_2$](SbF$_6$)$_2$) C, 25.41; H, 3.10; N, 5.39%.

2.11. Synthesis of catena-[μ-(N-(α-4-picolyl-1κN)morpholinyl-2κN′)silver(I)] hexafluoridoantimonate(V) hemi(tetrahydrofuran) (complex poly-[Ag(L2)]SbF₆·0.5THF 7) and bis-[μ-(N-(α-4-picolyl-1κN)morpholinyl-2κN′)-bis-tetrahydrofuranatosilver(I)] hexafluoridoantimonate(V)] (complex [Ag₂(L2)₂(THF)₄](SbF₆)₂ 8)

L2 (11 mg, 0.062 mmol) was dissolved in THF (2 mL). AgSbF$_6$ (18 mg, 0.052 mmol) was dissolved in THF (2 mL) and the two solutions were combined and left in a sealed vial which was wrapped in foil. After two days, colorless crystals formed and were isolated by filtration. Yield 11 mg (33%); m.p. 155-157 °C (decomp.); v_{max}/cm^{-1} (ATR): 2963 w br, 2858 w, 2822 w, 2755 w, 1619 s, 1564 w, 1467 w, 1458 m, 1450 m, 1431 s, 1400 m, 1363 w, 1346 m, 1335 m, 1309 w, 1296 s, 1267 s, 1245 w, 1234 m, 1212 w, 1136 s, 1128 s, 1113 s, 1100 m, 1088 s, 1066 s, 1058 s, 1031 m, 1025 m, 992 s, 975 m, 923 s, 893 w, 870 s, 840 m, 822 s, 795 s, 742 w, 649 s, 646 s. Elemental analysis suggests partial loss of lattice THF on drying in air; Found C, 26.25; H, 3.19; N, 5.07%; calculated for $C_{24}H_{36}N_4O_3F_{12}Sb_2Ag_2$ ([Ag$_2$(**L2**)$_2$(THF)](SbF$_6$)$_2$), C, 25.83; H, 3.25; N, 5.02%. X-ray powder diffraction confirms that the bulk phase consists of the discrete species **8** with **7** occurring only as a trace impurity.

2.12. Synthesis of catena-[μ-(N-(α-4-picolyl-1κN)piperidinyl-2κN′)-μ-trifluoroacetato-κO;κO-silver(I)] (complex poly-[Ag(L1)(CO₂CF₃)] 9)

L1 (11 mg, 0.063 mmol) was dissolved in THF (3 mL). AgCO$_2$CF$_3$ (7.0 mg, 0.032 mmol) was dissolved in THF (3 mL) and the two solutions were combined and left in a sealed vial which was wrapped in foil. After four days, colorless crystals had formed and were isolated by filtration. Yield 6.2 mg (49%); m.p. 165 − 168 °C (decomp.); v_{max}/cm^{-1} (ATR): 2979 w, 2945 w, 2923 w, 2847 w, 2831 w, 2779 w, 1660 s, 1610 s, 1594 m, 1557 w, 1496 w,
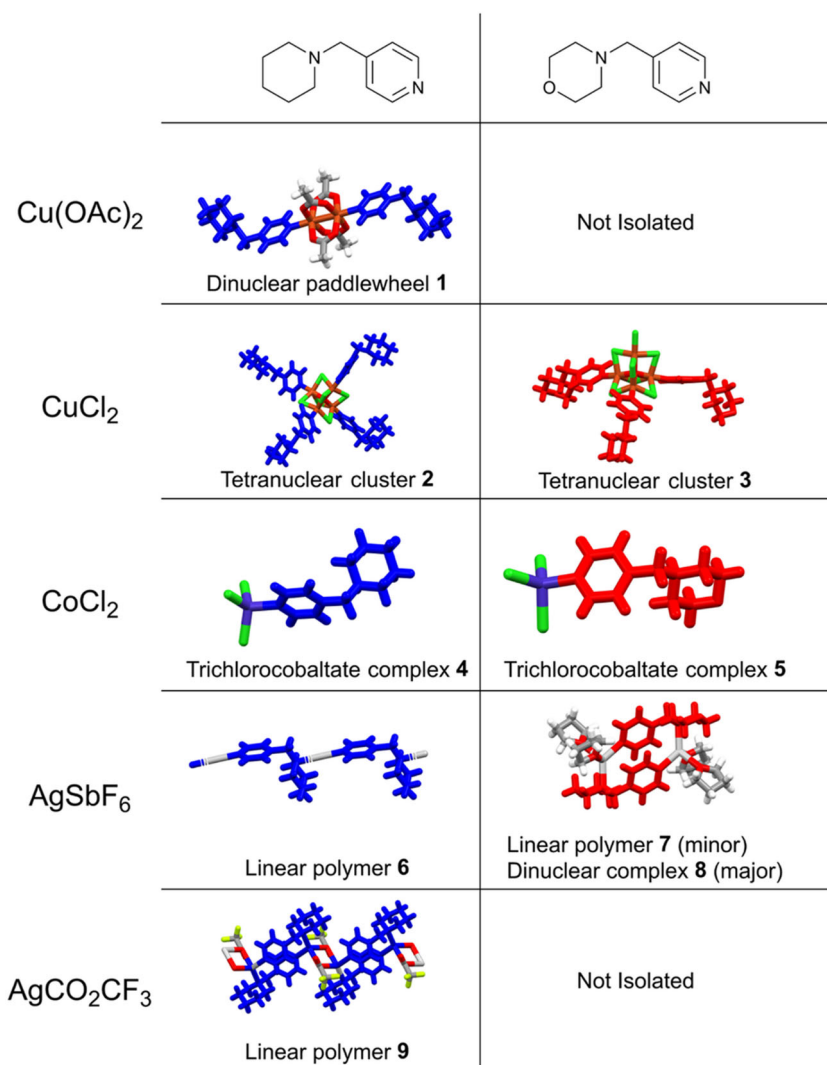
Figure 1. Summary of the coordination behaviors observed in **1-9** and the role of ligands **L1** (left column, blue) and **L2** (right column, red) within their structures.

1474 w, 1461 w, 1425 w, 1423 m, 1410s, 1387 w, 1375 w, 1348 w, 1326 w, 1302 m, 1279 w, 1223 m, 1213 m, 1192s, 1170s, 1115s, 1100s, 1083 m, 1064 m, 1060 m, 1008 m, 982 m, 979 m, 920 m, 872 w, 865 m, 854 s, 816 s, 815 s, 782 s, 780 s, 724 m, 720 s, 616 s, 606 w; Found C, 39.48; H, 3.94; N, 6.94%; calculated for $C_{13}H_{16}N_2O_2F_3Ag$, C, 39.32; H, 4.06; N, 7.05%.

3. Results and discussion

Copper(II) and cobalt(II) give coordination complexes in which the resulting geometry is largely controlled by geometric constraints imparted by the metal ion, which can be used to reliably engineer metal-organic species from various reproducible building units [28]. These ions were chosen to generate complexes in which the piperidine or
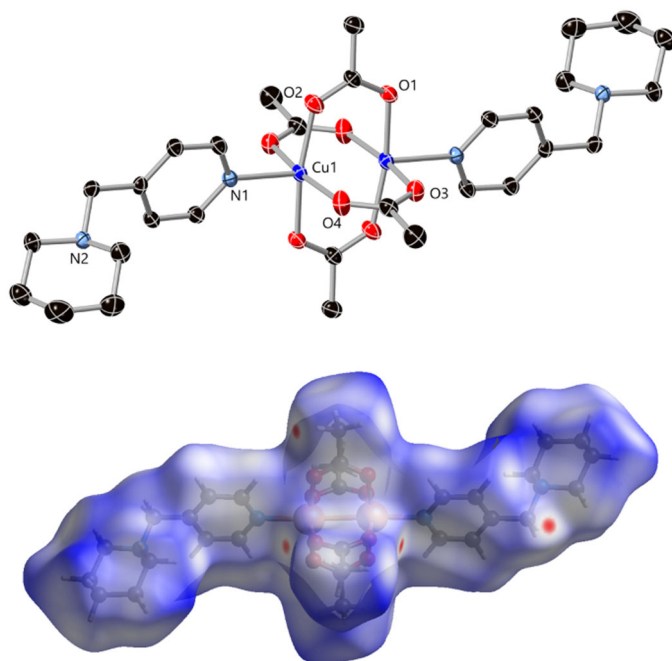
Figure 2. (Top) Structure of **1** with labeling scheme for unique heteroatoms. ADPs are rendered at the 50% probability level and hydrogen atoms are omitted for clarity. (Bottom) Normalized contact surface mapping of the Hirshfeld surface showing the two C–H···O donor/acceptor pairs as the only notable features at the visualization level $-0.1/+1.5$ Å.

morpholine functionalities of **L1** and **L2** were remote from the metal ion, and able to influence crystal packing behavior separate from the geometric preferences of the coordination sphere. On the other hand, silver(I) is a much softer metal ion with a closed shell d^{10} electron configuration, and a much more flexible coordination geometry [29]. The typically lower coordination number of silver(I) promotes coordination through sterically hindered tertiary amines as well as pyridine donors, and based on numerous examples of silver complexes of piperidine and piperazine-containing ligands [30] our expectation was for **L1** and **L2** to act as bridging ligands in these complexes.

The extra oxygen in the morpholine ring of **L2** serves two functions as a crystal engineering tecton, as both a hydrogen bond acceptor and by polarizing the nearby C–H groups. The electronic differences between the two cycles are evident from the pKa of their conjugate acids (10.08 for N-methylpiperidine *vs.* 7.41 for N-methylmorpholine) [31]. As such, **L2** would be expected to be less active for coordination through the nitrogen atom [32], but to show greater tendencies as a C–H hydrogen bond donor. With these design principles in mind, nine new coordination compounds were crystallized containing **L1** and **L2**, as summarized in Figure 1.

3.1. Copper(II) complexes

Combination of **L1** and **L2** with copper(II) salts resulted in discrete coordination complexes. In each case only the pyridyl nitrogen of the ligand coordinates to a copper(II)
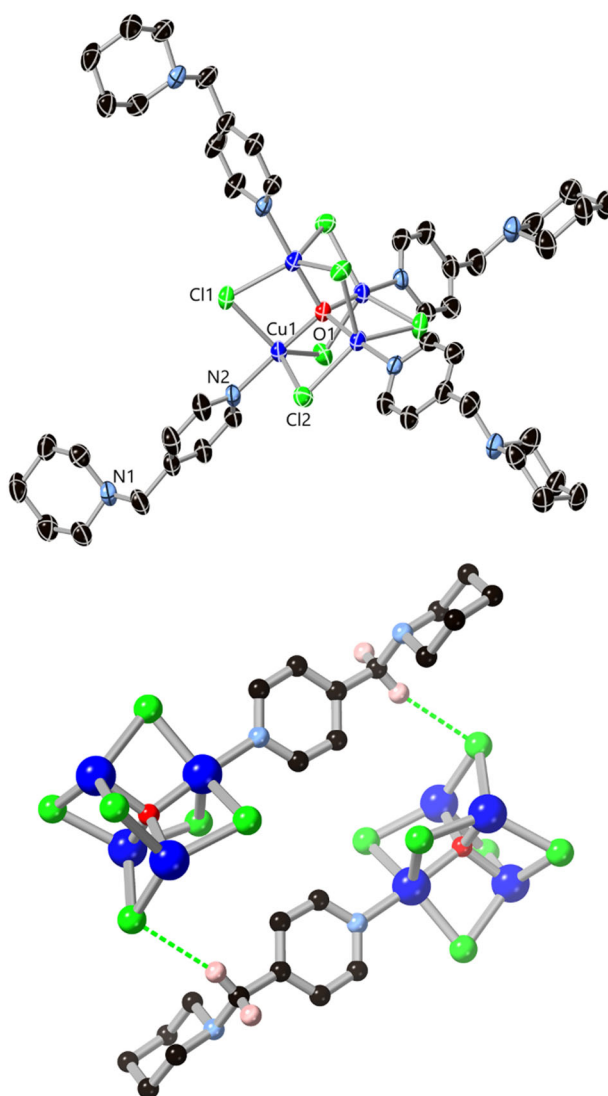
Figure 3. (Top) Structure of **2** with labeling scheme for unique heteroatoms. ADPs are rendered at the 50% probability level and hydrogen atoms and disordered lattice solvent molecules are omitted for clarity. (Bottom) The reciprocated C–H···Cl interaction between two complexes in the structure of **2**.

ion. In the case of copper acetate dihydrate, a discrete dinuclear complex, [Cu$_2$(OAc)$_4$(**L1**)$_2$] (**1**), was generated by reaction with **L1** in acetonitrile, while no equivalent **L2** complex could be crystallized under comparable conditions. The diffraction data for **1** were solved and refined in the monoclinic space group $P2_1/n$, and the structural model consists of a centrosymmetric dinuclear copper acetate paddlewheel with two **L1** molecules coordinating to the axial sites of the copper(II) ions, *via* the pyridyl nitrogen atoms, shown in Figure 2. The copper(II) ion has a square pyramidal geometry with a long axial Cu-N bond of 2.148(2) Å compared to the equatorial Cu-O bonds of 1.966(2)-1.969(2) Å.

Complex **1** contains no conventional hydrogen bond donors, but analysis of the normalized contact distance mapping of the Hirshfeld surface reveals two types of directional H···O contacts involving the acetate oxygen atoms O3 and O4 (Figure 2). These interactions originate at the two most polarized C–H groups, namely the picolyl methylene group and acetato methyl group, with C···O distances of 3.478(4) Å and 3.561(4) Å, respectively. Besides these interactions, the fingerprint plot contains no other significant features (ESI, Figure S9); there are no substantial $\pi \cdots \pi$ contacts in the structure of **1**, with the remaining crystal packing influences largely consisting of diffuse C···H and H···H contacts.

The reaction of **L1** and **L2** with $CuCl_2 \cdot 2H_2O$ again resulted in discrete coordination complexes **2** and **3**, respectively. While **L1** produced isostructural materials on reaction with copper(II) chloride in either methanol or acetonitrile, crystalline material could only be reliably generated from **L2** when using acetonitrile as the solvent.

In both cases, the pyridyl ligands cap tetranuclear μ_4-oxo clusters. Equivalent pyridyl-capped tetranuclear copper(II) clusters have been previously reported and have been of crystallographic and magnetochemical interest [33]. For **L1**, the cluster (**2**) takes the form $[Cu_4(\mu_4\text{-}O)(\mu_2\text{-}Cl)_6(\textbf{L1})_4]$ in the tetragonal space group $I4_1/a$, as shown in Figure 3. The asymmetric unit contains one ligand molecule, one copper(II) ion, two chlorido ligands and one oxo ligand, with the anionic species each occupying crystallographic special positions. Diffraction-quality crystals were obtained by crystallization in methanol. While this method gave higher quality single crystals, the bulk material for analysis is more reliably crystallized from acetonitrile, and X-ray powder diffraction confirms this material is isostructural to the methanol solvate (ESI, Figure S2). Elemental analysis suggests lattice water is present in the acetonitrile form which likely fulfills the same structural role as methanol. One disordered methanol molecule was detected within the asymmetric unit, and further modeling of small amounts of additional disordered solvent coincident with the symmetry elements did not yield any improvements to the structural model.

The cluster core conforms to the typical geometry observed for tetrahedral $[Cu_4OCl_6]$ clusters; the copper ion adopts a distorted trigonal bipyramidal geometry ($\tau_5 = 0.4$) [34], with Cu-Cl distances of 2.3492(9) − 2.4994(9) Å and axial Cu-N and Cu-O distances of 1.979(3) and 1.9068(4) Å, respectively. All Cu···Cu distances are equivalent at 3.1241(6) Å. The primary intermolecular contacts in the structure of **2** involve the lattice solvent molecules and are somewhat obscured due to the disorder inherent in these molecules; as such, the Hirshfeld surface is less instructive. The **L1** ligand acts as a hydrogen bond acceptor for the lattice methanol molecule at the piperidine nitrogen atom and also donates C–H ···O hydrogen bonds from the methylene and pyridyl C–H groups to the methanol molecule. However, closer inspection of the fingerprint plot (ESI, Figure S10) reveals the presence of additional symmetric features consistent with direct interactions between the two clusters. The most significant of these involves the bridging chlorido ligand Cl2 and the methylene carbon atom C6, with a C···Cl distance of 3.784(4) Å and C–H···Cl angle of 165.2(2)° (Figure 2).

Repeating the reaction with **L2**, a similar μ_4-oxo tetranuclear cluster is observed, however in $[Cu_4OCl_7(\textbf{L2})_2(\textbf{L2H})]$ (**3**) one of the four capping ligand molecules is replaced with a terminal chlorido ligand. This results in a net negative charge for the
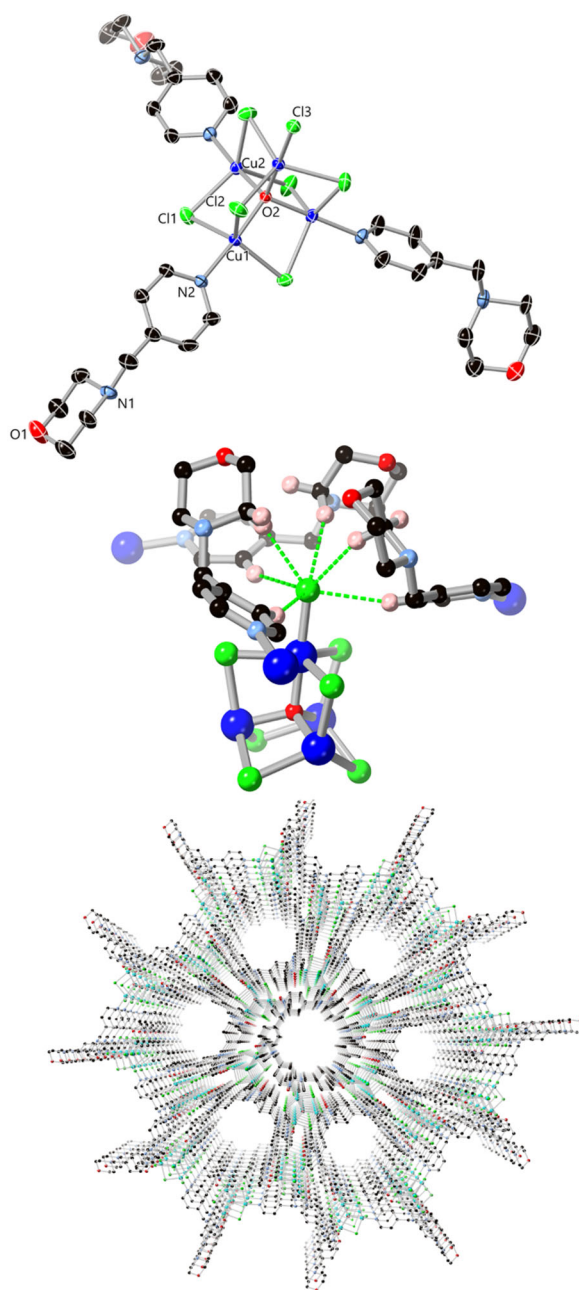
Figure 4. (Top) Structure of **3** with labeling scheme for unique heteroatoms. ADPs are rendered at the 50% probability level and hydrogen atoms and lattice solvent molecules are omitted for clarity. (Centre) The C–H···Cl contacts which encapsulate the terminal chlorido ligand in the structure of **3**. (Bottom) Extended structure of **3** showing the linear hexagonal channels parallel to the *c* axis.

cluster core; we ascribe charge balance to (crystallographically disordered) protonation on one of the three equivalent morpholine groups. We found the synthesis for **3** could be performed in pure acetonitrile, but due to variations in water content a more reliable synthesis is achieved by addition of *ca.* 0.5% H_2O. The diffraction data for **3** were

solved and refined in the trigonal space group P-3. The asymmetric unit contains two copper ions, one monodentate **L2H** molecule, a μ_4 oxo ligand, two μ_2 chlorido ligands and a terminal chlorido ligand, as shown in Figure 4. The crystallographic threefold axis is coaxial with the O2-Cu2-Cl3 vector, with the three **L2** molecules symmetrically distributed around the core. One lattice water molecule was unambiguously located from the Fourier residuals, while additional solvation within the primary solvent channels, heavily disordered and coincident with symmetry elements, was accounted for using a solvent mask. Copper(II) ions Cu1 and Cu2 adopt more regular trigonal bipyramidal geometries ($\tau_5 = 0.15$ and 0.00, respectively) [34] compared to **2**, although both Cu-N (1.966(3) Å) and Cu-O distances (1.9009(13) and 1.907(4) Å), and Cu⋯Cu distances (3.0935(7) and 3.1196(7) Å for Cu1-Cu1 and Cu1-Cu2, respectively) are essentially equivalent to those described above. As expected, the terminal chlorido ligand exhibits a shorter Cu-Cl distance of 2.2292(15) Å compared to the bridging chlorido ligands (2.3797(9) − 2.4254(9) Å).

Each complex assembles around hexagonal solvent channels in the extended structure of **3**. The crystallographically-resolved lattice water molecule is located within a typical hydrogen bonding distance of 2.924(4) Å from the morpholine nitrogen; as only one of every three of these groups is protonated, the oxygen takes the same position as either a hydrogen bond donor or acceptor. While the disordered nature of the classical hydrogen bonding interaction involving the morpholine nitrogen atom and the presence of solvent channels without discrete atom positions complicates analysis of the Hirshfeld surface, a series of C–H⋯Cl and C–H⋯O interactions are evident in the fingerprint plot (ESI, Figure S11). Most notably, the terminal chlorido ligand undergoes close contacts with three adjacent **L2** units, which each interact through the pyridyl C–H group C10 and a morpholine ring CH$_2$ group C14, with shorter C⋯Cl distances and similar C–H⋯Cl angles to those seen in **2** (3.653(3) and 3.686(4) Å, 157.5(2) and 155.3(2)°, respectively). Each morpholine ring further undergoes a dimer-type interaction, with relatively short C⋯O distances of 3.261(5) Å offset by a smaller than ideal C–H⋯O angle of 143.5(3)°.

The hexagonal solvent channels within the structure are approximately 10.6 Å in diameter. Initial analysis into the possibility of guest adsorption into this material was carried out *via* thermogravimetric analysis (ESI Figure S19), which revealed a continuous gradual mass loss blending into a more rapid onset of decomposition at 210 °C, at a ramp rate of 5 °C/min. Given the lack of an obvious plateau in the trace we attempted to gently activate the solid by extended heating of the material under dynamic vacuum overnight at 80 °C. However, even these mild activation conditions still led to eventual decomposition with visible amorphization over 12 h, suggesting that the solvent channels are not readily accessible for guest uptake. This observation implies that the inter-cluster contacts do not provide sufficient stabilization to support the framework when the diffuse solvent is removed.

3.2. Cobalt(II) complexes

The reaction of either **L1** or **L2** with cobalt(II) chloride hexahydrate in acetonitrile gave structurally related complexes **4** and **5**, respectively, with the general formula
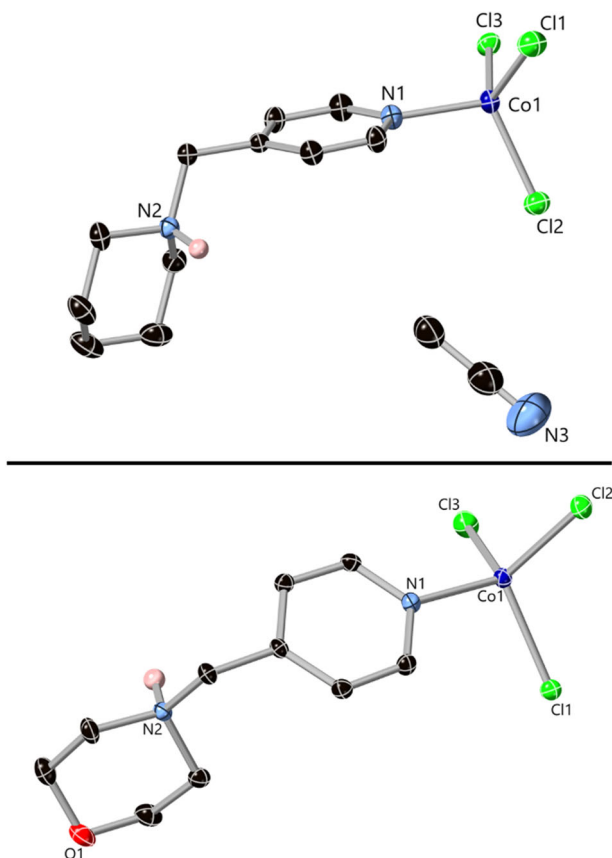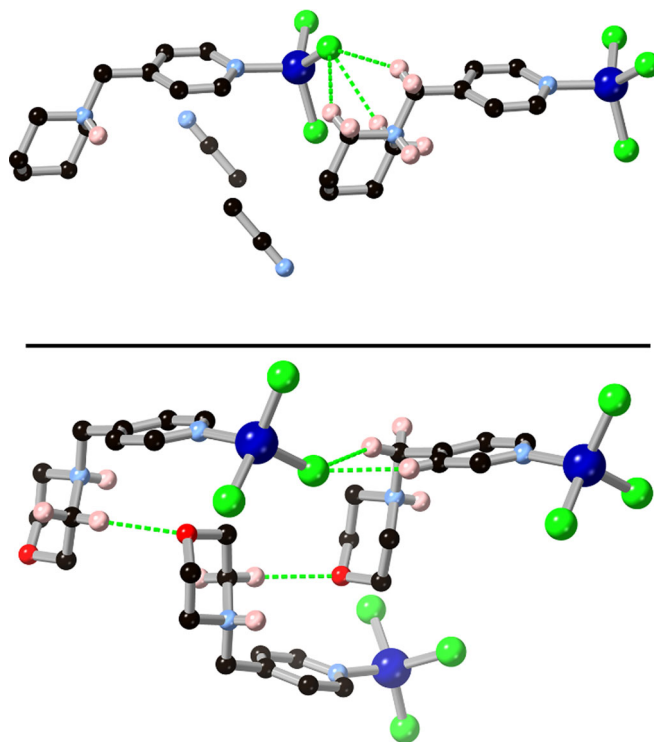
Figure 5. Structures of **4** (top) and **5** (bottom) with heteroatom labeling scheme. ADPs are rendered at the 50% probability level and selected hydrogen atoms are omitted for clarity.

[CoCl$_3$(**HL**)]. In both complexes, coordination occurs solely through the pyridine nitrogen atom with protonation on the amine for charge balance. The metal coordination sphere is essentially equivalent in both cases, and so these materials make for a more straightforward investigation of the intermolecular interactions based on the amine substitution pattern.

The diffraction data for [CoCl$_3$(**L1H**)]·MeCN (**4**) were solved and refined in the monoclinic space group $P2_1/c$. The asymmetric unit consists of a protonated **L1H** ligand coordinating to a tetrahedral cobalt(II) ion with three terminal chloride ligands completing its coordination sphere, and one non-coordinating acetonitrile molecule. For [CoCl$_3$(**L2H**)] (**5**), solved and refined in the monoclinic space group $P2_1/n$, the basic structure of the complex is equivalent, except no solvent molecules are present within the lattice. The structures of **4** and **5** are shown in Figure 5. In both cases, X-ray powder diffraction (ESI Figures S4 and S5) confirms that only a single phase is present within each bulk material, consistent with elemental analysis data which show that only **4** has the acetonitrile solvate.

In both complexes, the N–H···Cl hydrogen bonding is the most obvious intermolecular interaction (ESI, Figure S18). This takes the form of a linear chain, with a helical form in **4** and a zig-zag form in **5**, with a shorter N···Cl distance in the more acidic **5**

Figure 6. Comparison of the weak C–H⋯X interactions in the structures of **4** (top) and **5** (bottom). In **5**, a morpholine ring occupies the position otherwise occupied by lattice acetonitrile molecules in **4**, accompanied by modification in the C–H⋯Cl contacts between neighboring molecules.

(3.2007(17) and 3.1366(11) Å for **4** and **5**, respectively). When considering the weaker C–H contacts, more substantial differences are evident between **4** and **5**. In **4**, the most notable feature on the normalized contact distance map beyond the classical hydrogen bonds is a tridentate contact from the three methylene groups adjacent to the piperidine nitrogen. The three axial hydrogen atoms from these positions are directed toward Cl1, with C⋯Cl distances of 3.669(2) − 3.721(2) Å and C–H⋯Cl angles from 145.91(12) − 148.59(11)°. No significant directional contacts are evident from the remainder of the piperidine ring.

In contrast, in **5** a similar chelating C–H⋯Cl contact only involves the linking methylene group and a pyridyl C–H group, with similar C⋯Cl distances (3.6394(13) and 3.5704(12) Å) and C–H⋯Cl angles (150.65(8) and 154.30(8)°, respectively). This is complemented by a C–H⋯O contact between the morpholine oxygen and the ring methylene group adjacent to the nitrogen atom (C⋯O distance 3.5185(18) Å). This interaction accompanies the association of the morpholine group into the cleft between the two ring moieties on **L2** which, in the case of **4**, is instead occupied by the weakly associating acetonitrile molecule, as shown in Figure 6. Given the other structural similarities between the two complexes, these interactions involving the morpholine oxygen are presumably significant in establishing the solvatomorphism between **4** and **5**.
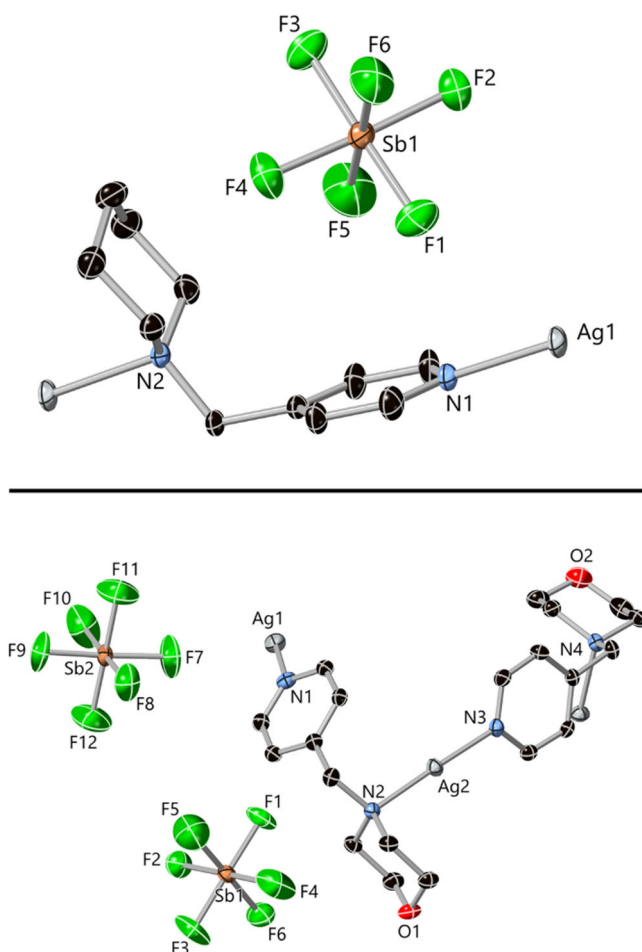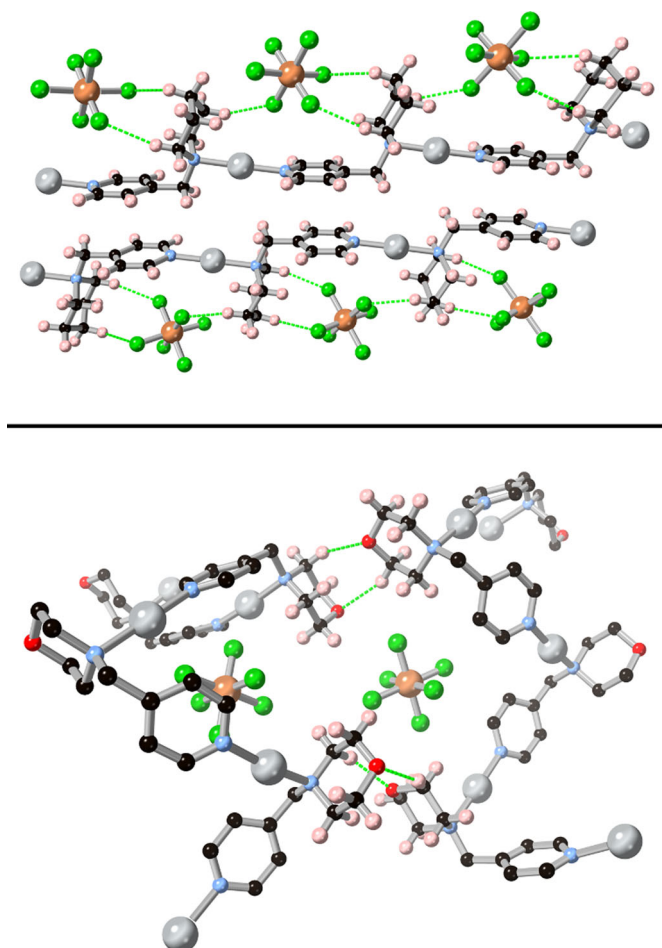
Figure 7. Structures of **6** (top) and **7** (bottom) with labeling scheme for unique heteroatoms. ADPs are rendered at the 50% probability level and hydrogen atoms and disordered solvent molecules are omitted for clarity.

3.3. Silver(I) complexes

In keeping with previous studies on silver(I) complexes with cyclic amine ligands [30], in all cases **L1** and **L2** coordinate to silver ions through both the pyridine and piperidine/morpholine nitrogen atoms. Combination of $AgSbF_6$ with **L1** or **L2** in THF gave structurally related one-dimensional coordination polymers, allowing for direct comparison of the ligand backbones and their contribution to the extended structure. As shown in Figure 7, both complexes take the empirical formula *poly*-[Ag(**L**)]SbF$_6$·0.5THF, though *poly*-[Ag**L1**]SbF$_6$·0.5THF (**6**) crystallizes with a single formula unit within the asymmetric unit, while the asymmetric unit of *poly*-[Ag(**L2**)]SbF$_6$·0.5THF (**7**) contains two unique ligand molecules, silver ions and hexafluoroantimonate counterions. In both cases the silver ions adopt linear two-coordinate geometries bound by one pyridine and one tertiary amine, with the pyridine typically giving the shorter Ag-N distance (2.114(3) − 2.121(3) Å *vs.* 2.170(3) − 2.181(3) Å), and no significant difference between the two complexes in these values.

Figure 8. Comparison of the interaction modes involving the amine rings in the structures of **6** (top) and **7** (bottom). Complex **6** predominantly forms C–H⋯F contacts with the hexafluoroantimonate anions, while in **7** pairs of morpholine rings associate through C–H⋯O contacts.

The extended structures of the two complexes differ substantially in their geometries, as shown in Figure 8. The piperidine species **L1** forms a straightforward linear chain with one flat face, where π⋯π interactions between antiparallel pyridine rings are evident, and one notched face where hexafluoroantimonate anions are encapsulated between piperidine rings. This leads to various C–H⋯F contacts between the cationic chain and the discrete anions, although the shortest C⋯F distances (3.458(5) Å for C10⋯F1) involve the backbone ring methylene groups rather than the more acidic sites adjacent to the amine. This presumably relates to the steric influence of the pyridine ring, which itself exhibits a minimum F⋯mean plane distance of 3.03 Å with F1.

In stark contrast, **L2** lends a twisted zig-zag motif to the extended structure which substantially reduces the possible contact between the morpholine group and the hexafluoroantimonate anion. The anions engage in similar anion⋯π interactions to those in **6**, while adjacent morpholine groups associate through unsymmetric C–H⋯O contacts rather than forming any substantial contacts with the anions. Two
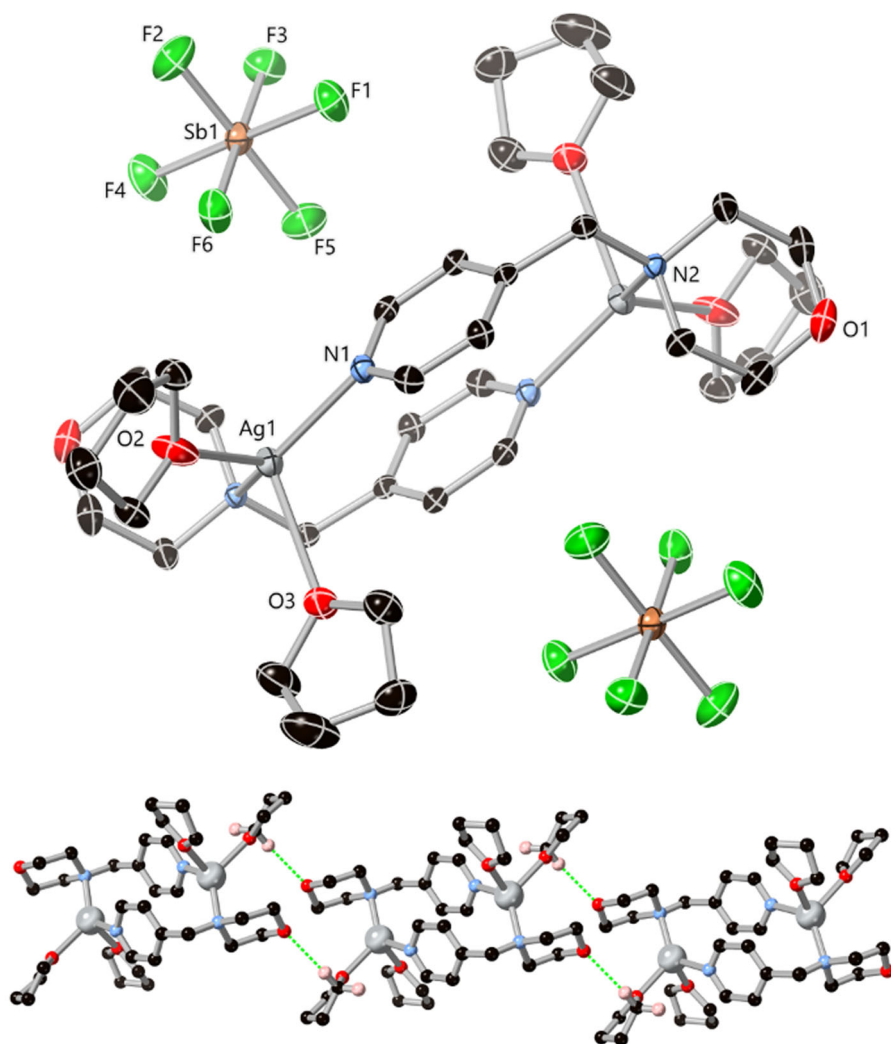
Figure 9. (Top) Structure of **8** with labeling scheme for unique heteroatoms. ADPs are rendered at the 50% probability level and hydrogen atoms are omitted for clarity. (Bottom) Intermolecular C–H⋯O between the coordinating THF methylene groups and non-coordinating morpholine oxygen atoms in the structure of **8**; selected hydrogen atoms and anions omitted for clarity.

nonequivalent morpholine rings associate through an $R_2^2(7)$ motif, with C⋯O distances of 3.398(5) and 3.331(5) Å and C–H⋯O angles of 154.8(3) and 154.9(3)°. Similar C–H⋯O contacts are observed between the morpholine rings and the disordered THF solvent molecules which are absent in the structure of **6**. The F⋯π and π⋯π contacts exhibit similar metrics to those in **6**, again implicating the association of adjacent morpholine rings in influencing the extended structure.

Examination of the X-ray powder diffraction pattern from a bulk sample of **7** shows that the polymeric species **7** is the minor product from this reaction and only occurs in trace quantities, albeit with high quality single crystals. After collecting another single crystal X-ray diffraction dataset, the discrete complex [Ag₂(**L2**)₂(THF)₄](SbF₆)₂ (**8**) was
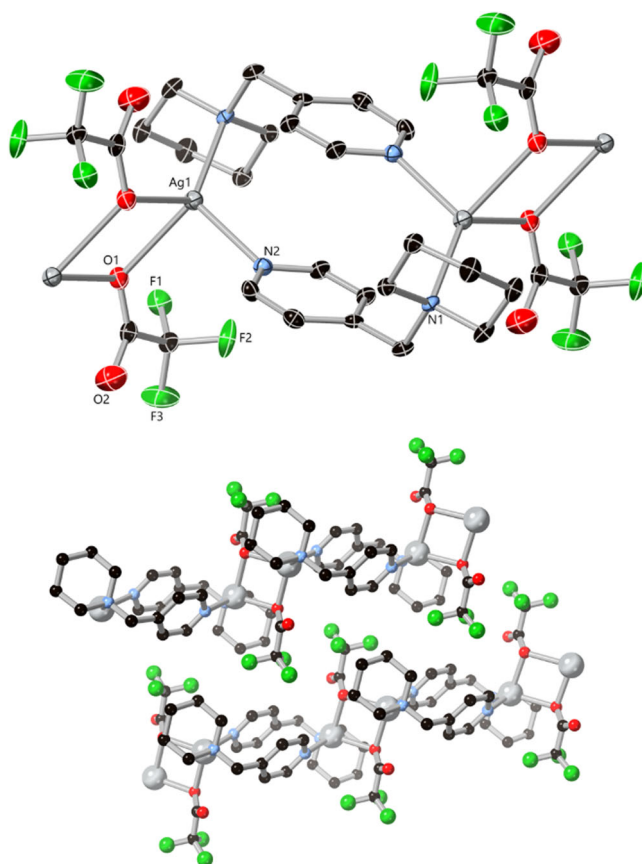
Figure 10. (Top) Structure of **9** with labeling scheme for unique heteroatoms. ADPs are rendered at the 50% probability level and hydrogen atoms are omitted for clarity. (Bottom) Interactions between two adjacent chains of **9** showing interdigitation of trifluoromethyl groups.

elucidated as the major product. Complex **8** is a discrete dinuclear complex. The diffraction data were solved and refined in the triclinic space group *P*-1 and the asymmetric unit, shown in Figure 9, consists of one ligand molecule coordinating to a silver(I) ion with two coordinating THF molecules and a non-coordinating hexafluoroantimonate anion. The complete structure of **8** is a centrosymmetric, dinuclear M_2L_2 "box," with the silver ion adopting a four-coordinate pseudo-tetrahedral ($\tau_4 = 0.73$) [35] geometry. The angle N1-Ag1-N2 is the largest in the coordination sphere, but at 129.80(7)° this is far from the linear angle observed in the previous complexes. Both Ag-N distances (2.284(2) and 2.2976(19) Å for N1 and N2, respectively) are longer than those in **6** and **7**, consistent with the higher coordination number. Similar coordination geometries have been observed in silver complexes of 4-aminomethylpyridine by Feazell *et al.* and Sailaja *et al.*, all of which are polymeric [36]. These observations suggest a general preference for this coordination environment in silver 4-picolylamine complexes, although we saw no evidence for a second phase of this type in the equivalent **6**.

With all the lattice THF molecules involved in metal coordination, the only available Lewis basic sites in **8** are the morpholine oxygen and the hexafluoroantimonate

fluorine atoms. Adjacent complexes associate into linear chains through C–H⋯O inter-actions between the morpholine oxygen atoms and a ring methylene group of a THF species (with a C⋯O distance of 3.369(4) Å and a C–H⋯O angle of 145.40(16)°), which accounts for the main symmetric feature off the diagonal in the fingerprint plot (ESI, Figure S16). The hexafluoroantimonate anion also accepts several C–H⋯F contacts from the bridging methylene group, coordinating THF molecules and pyridyl C–H groups. Despite externally-facing π surfaces, intermolecular π⋯π interactions in the structure of **8** are minimal due to poor overlap between adjacent rings, likely relating to the steric constraints of the coordination sphere. The intramolecular π⋯π contact within the dinuclear box exhibits a short interplanar distance of 3.26 Å, although the overlap between the two rings is reduced by a lateral slip of 2.37 Å.

To consider the geometric influence of a coordinating anion, the reaction was repeated with silver trifluoroacetate in THF. Single crystals were only forthcoming for **L1**, no crystalline material could be isolated for the equivalent **L2** species. The diffrac-tion data for $poly$-[Ag**L1**]CO$_2$CF$_3$ (**9**) were solved and refined in the monoclinic space group $P2_1/c$, revealing a one-dimensional polymeric chain as seen in Figure 10. The structure consists of similar dinuclear Ag$_2$L$_2$ boxes as observed in **8**, but with tetrahe-dral coordination spheres completed by two μ$_2$ acetato oxygen atoms which bridge each dinuclear species into a polymeric assembly. The silver ions adopt a similarly distorted tetrahedral coordination sphere as seen in **8** ($\tau_4 = 0.75$) [35], with a small O1-Ag1-O1′ angle of 80.14(5)° for the four-membered Ag$_2$O$_2$ ring. Due to the steric hindrance around the trifluoroacetato oxygen atoms from the nearby coordination spheres, and the lack of any other Lewis basic sites in the structure, the extended structure of **9** is devoid of any significant C–H⋯X contacts and mainly consists of tri-fluoroacetate groups interdigitating in the clefts of adjacent chains. The inter-chain interactions appear mainly governed by diffuse C–H⋯π contacts and other dispersion-type interactions.

4. Conclusion

A series of nine new discrete and polymeric coordination compounds of two structur-ally related picolylamine ligands were prepared, with the goal of establishing the influ-ence of weak C–H⋯X contacts from the amine backbone on the extended structures. The copper(II) and cobalt(II) species **1**-**5** and silver(I) complex **8** exist as discrete com-plexes, while three polymeric complexes **6**, **7** and **9** were prepared. We note a consist-ent tendency for the morpholine substituents to favor the formation of dimers or homoleptic chains through weak C–H⋯O interactions, with the potential to disrupt other modes of association.

Switching from piperidine to morpholine in the copper complexes **2** and **3** led to wholesale structural changes, where the piperidine ligand **L1** favors the T$_d$ symmetric Cu$_4$OCl$_6$(**L1**)$_4$ cluster while the morpholine species instead gave the C$_3$ symmetric Cu$_4$OCl$_7$(**L2**)$_2$(**L2H**) core. Both complexes showed extensive weak interactions involving the amine backbones, but direct comparison was challenging given the other struc-tural changes. The cobalt complexes **4** and **5** provided more direct evidence as to the role of the morpholine oxygen on the extended structure, where solvatomorphism

accompanied by a change in bridging geometry is observed alongside variation in C–H···X interactions. A similar effect is observed in the silver complexes **6** and **7**, where the modes of interaction between the polymeric cation and discrete anions are impacted based on the presence of the oxygen atom in the cyclic amine backbone. In most cases, clear preference for the most polarized methylene donors adjacent to the protonated or coordinating amine nitrogen atom was observed in these systems, except where these contacts were prohibited on steric grounds.

These observations provide new starting points for designing divergent ligands for coordination polymers and related materials in which non-classical hydrogen bonding interactions can be controlled to enhance the effect of stabilizing intermolecular contacts. Perhaps equally important is the notion of designing materials in which these contacts are avoided. The growing popularity of aliphatic benzene isosteres in crystalline materials may give new opportunities for minimizing the packing density, and enhancing pore volume and selectivity for hydrophobic guests by designing materials lacking in polarized C–H donors and modes of alkylamine aggregation.

Disclosure statement

No potential conflict of interest was reported by the authors.

References

[1] (a) E.A. Dolgopolova, A.M. Rice, C.R. Martin, N.B. Shustova. *Chem. Soc. Rev.*, 47, 4710 (2018). (b) S. Suárez-García, R. Solórzano, R. Alibés, F. Busqué, F. Novio, D. Ruiz-Molina. *Coord. Chem. Rev.*, 441, 213977 (2021). (c) J. Xue, X. Hang, J. Ding, B. Li, R. Zhu, H. Pang, Q. Xu. *Coord. Chem. Rev.,* 430, 213656 (2021). (d) N. Hanikel, M.S. Prévot, O.M. Yaghi. *Nature Nanotech.*, 15, 348 (2020).

[2] (a) C.B. Aakeröy, M. Fasulo, N. Schultheiss, J. Desper, C. Moore. *J. Am. Chem. Soc.*, 129, 13772 (2007). (b) C.B. Aakeröy, M. Fasulo, N. Schultheiss, J. Desper, C. Moore. *J. Am. Chem. Soc.,* 129, 13772 (2007). (c) G.M. Espallargas, F. Zordan, L.A. Marin, H. Adams, K. Shankland, J. van de Streek, L. Brammer. *Chem. Eur. J.,* 15, 7554 (2009).

[3] H. Jiang, D. Alezi, M. Eddaoudi. *Nat. Rev. Mater.*, 6, 466 (2021).

[4] (a) A.K. Ghosh, A. Hazra, A. Mondal, P. Banerjee. *Inorg. Chim. Acta*, 488, 86 (2019). (b) L. Brammer, G.M. Espallargas, S. Libri. *CrystEngComm.*, 10, 1712 (2008). (c) M. Borovina, I. Kodrin, M. Đaković. *CrystEngComm.*, 20, 539 (2018). (d) C.S. Hawes. *Dalton Trans.*, 50, 6034 (2021). (e) M.C. Pfrunder, A.J. Brock, A.S. Micallef, J.K. Clegg, J. McMurtrie. *Cryst. Growth Des.*, 19, 5334 (2019).

[5] Y. Gu, T. Kar, S. Scheiner. *J. Am. Chem. Soc.*, 121, 9411 (1999).

[6] (a) S. Scheiner. *J. Phys. Chem. B*, 109, 16132 (2005). (b) U. Koch, P.L.A. Popelier. *J. Phys. Chem.*, 99, 9747 (1995).

[7] (a) S.L. Price. *CrystEngComm.*, 6, 344 (2004). (b) M.A. Spackman, J.J. McKinnon. *CrystEngComm.*, 4, 378 (2002).

[8] I. Dance, M. Scudder. *CrystEngComm.*, 11, 2233 (2009). doi:10.1039/b904479e

[9] (a) I. Hisaki, C. Xin, K. Takahashi, T. Nakamura. Angew. *Chem. Int. Ed.*, 131, 11278 (2019). (b) P. Muang-Non, H.D. Toop, C.J. Doonan, N.G. White. *Chem. Commun.*, 58, 306 (2021). (c) P. Li, M.R. Ryder, J.F. Stoddart. *Acc. Mater. Res.,* 1, 77 (2020). (d) Y. Li, S. Tang, A. Yusov, J. Rose, A.N. Borrfors, C.T. Hu, M.D. Ward. *Nature Commun.*, 10, 4477 (2019). (e) J. Marti-Rujas, L. Colombo, J. Lu, A. Dey, G. Terraneo, P. Metrangolo, G. Pilati, G. Resnati. *Chem. Commun.*, 48, 8207 (2012). (f) V.I. Nikolayenko, D.C. Castell, D.P. van Heerden, L.J. Barbour. *Angew. Chem. Int. Ed.*, 57, 12086 (2018).

[10] (a) A.A. Tehrani, A. Morsali, M. Kubicki. *Dalton Trans.*, 44, 5703 (2015). (b) G. Mahmoudi, *A. Morsali. Cryst. Growth Des.*, 8, 391 (2008).

[11] (a) V.S. Bryantsev, B.P. Hay. *J. Am. Chem. Soc.*, 127, 8282 (2005). (b) S. Lee, C.-H. Chen, A.H. Flood. *Nature Chem.*, 5, 704 (2013). (c) K.M. Mullen, J. Mercurio, C.J. Serpell, P.D. Beer. *Angew. Chem. Int. Ed.*, 48, 4781 (2009). (d) A.F. Henwood, I.N. Hegarty, E.P. McCarney, J.I. Lovitt, S. Donohoe, T. Gunnlaugsson. *Coord. Chem. Rev.*, 449, 214206 (2021).

[12] A.J. Emerson, A. Chahine, S.R. Batten, D.R. Turner. *Coord. Chem. Rev.*, 365, 1 (2018). doi:10.1016/j.ccr.2018.02.012

[13] L.A. Darunte, K.S. Walton, D.S. Sholl, C.W. Jones. *Curr. Opin. Chem. Eng.*, 12, 82 (2016). doi:10.1016/j.coche.2016.03.002.

[14] (a) M. Kalaj, S.M. Cohen.*ACS Cent. Sci.*, 6, 1046 (2020). (b) N. Planas, A.L. Czubak, R. Poloni, L.-C. Lin, A. McManus, T.M. McDonald, J.B. Neaton, J.R. Long, B. Smit, L. Gagliardi. *J. Am. Chem. Soc.*, 135, 7402 (2013). (c) A. Justin, J. Espin, I. Kochetygov, M. Asgari, O. Trukhina, W.L. Queen. *Inorg. Chem.*, 60, 11720 (2021).

[15] (a) A.Y. Chahine, A.L. Chaffee, G.P. Knowles, D.R. Turner, S.R. Batten. *CrystEngComm*, 24, 3416 (2022). (b) C. Hua, B.F. Abrahams, D.M. D'Alessandro. *Cryst. Growth Des.*, 16, 1149 (2016). (c) X. Qiao, Y. Ge, Y. Li, Y. Niu, B. Wu. *ACS Omega*, 4, 12402 (2019). (d) H. Hahm, H. Ha, S. Kim, B. Jung, M.H. Park, Y. Kim, J. Heo, M. Kim. *CrystEngComm*, 17, 5644 (2015). (e) C.S. Hawes, N.F. Chilton, B. Moubaraki, G.P. Knowles, A.L. Chaffee, K.S. Murray, S.R. Batten, D.R. Turner. *Dalton Trans.*, 44, 17494 (2015).

[16] (a) R. Kant, S. Maji.*Dalton Trans.*, 50, 785 (2021). (b) D.P. Martin, M.A. Braverman, R.L. LaDuca. *Cryst. Growth Des.*, 7, 2609 (2007). (c) A.R. LaDuca, R.L. LaDuca. *CrystEngComm.*, 20, 5677 (2018). (d) K. Kadota, Y.-I. Hong, Y. Nishiyama, E. Sivaniah, D. Packwood, S. Horike. *J. Am. Chem. Soc.*, 143, 16750 (2021). (e) A. Das, M. Choucair, D.P. Southon, J.A. Mason, M. Zhao, C.J. Kepert, A.T. Harris, D.M. D'Alessandro. *Microporous Mesoporous Mater.*, 174, 74 (2013). (f) Q. Mu, H. Wang, L. Li, C. Wang, Y. Wang, X. Zhao. *Chem. Asian J.*, 10, 1864 (2015). (g) M.T. Wharmby, J.P.S. Mowat, S.P. Thompson, P.A. Wright. *J. Am. Chem. Soc.*, 133, 1266 (2011).

[17] V.D. Slyusarchuk, P.E. Kruger, C.S. Hawes. *ChemPlusChem.*, 85, 845 (2020).[32378813

[18] (a) H.A. Miller, N. Laing, S. Parsons, A. Parkin, P.A. Tasker, D.J. White. *J. Chem. Soc., Dalton Trans.*, 3773 (2000). (b) J.I. Lovitt, T. Gorai, E. Cappello, J.M. Delente, S.T. Barwich, M.E. Möbius, T. Gunnlaugsson, C.S. Hawes. *Mater. Chem. Front.*, 5, 3458 (2021). (c) Z. Szakács, S. Rousseva, M. Bojtár, D. Hessz, I. Bitter, M. Kállay, M. Hilbers, H. Zhang, M. Kubinyi. *Phys. Chem. Chem. Phys.*, 20, 10155 (2018).

[19] (a) V. Schramm. *Inorg. Chem.*, 17, 714 (1978). (b) J.C. Vantourout, H.N. Miras, A. Isidro-Llobet, S. Sproules, A.J.B. Watson. *J. Am. Chem. Soc.*, 139, 4769 (2017). (c) V. Stilinović, K. Užarević, I. Cvrtila, B. Kaitner. *CrystEngComm*, 14, 7493 (2012). (d) B. Modec, N. Podjed, N. Lah. *Molecules*, 25, 1573 (2020).

[20] A. Parkin, I.D.H. Oswald, S. Parsons. *Acta Crystallogr. B*, 60, 219 (2004).

[21] Bruker-AXS. *Bruker APEX-3*, Bruker-AXS Inc., Madison, WI (2016).

[22] Bruker-AXS. *SADABS 2016/2*, Bruker-AXS Inc., Madison, WI (2016).

[23] G.M. Sheldrick. *Acta Crystallogr. A Found Adv.*, 71, 3 (2015).

[24] G.M. Sheldrick. *Acta Crystallogr. C Struct. Chem.*, 71, 3 (2015).
[25] O.V. Dolomanov, L.J. Bourhis, R.J. Gildea, J.A.K. Howard, H. Puschmann. *J. Appl. Crystallogr.*, 42, 339 (2009).
[26] P. van der Sluis, A.L. Spek. *Acta Crystallogr. A Found Crystallogr.*, 46, 194 (1990).
[27] P.R. Spackman, M.J. Turner, J.J. McKinnon, S.K. Wolff, D.J. Grimwood, D. Jayatilaka, M.A. Spackman. *J. Appl. Crystallogr.*, 54, 1006 (2021).
[28] (a) Y. Yan, S. Yang, A.J. Blake, M. Schröder. *Acc. Chem. Res.*, 47, 296 (2014). (b) A.J. Gosselin, C.A. Rowland, E.D. Bloch. *Chem. Rev.*, 120, 8987 (2020). (c) J.J. Perry IV, J.A. Perman, M.J. Zaworotko. *Chem. Soc. Rev.*, 38, 1400 (2009).
[29] (a) M.A. Haj, C.B. Aakeröy, J. Desper. *New J. Chem.*, 37, 204 (2013). (b) M. Oh, C.L. Stern, C.A. Mirkin. *Inorg. Chem.*, 44, 2647 (2005). (c) G. Lamming, J. Kolokotroni, T. Harrison, T.J. Penfold, W. Clegg, P.G. Waddell, M.R. Probert, A. Houlton. *Cryst. Growth Des.,* 17, 5753 (2017).
[30] (a) Y. Yilmaz, E. Soyer, O. Büyükgüngör. *Polyhedron*, 29, 920 (2010). (b) D. Das, K. Biradha. *Inorg. Chem. Front.,* 4, 1365 (2017). (c) S. Roy, H.M. Titi, B.K. Tripuramallu, N. Bhunia, R. Verma, I. Goldberg. *Cryst. Growth Des.*, 16, 2814 (2016). (d) L.J. Beeching, C.S. Hawes, D.R. Turner, S.R. Batten. *CrystEngComm,* 16, 6459 (2014). (e) C.S. Hawes, S.E. Hamilton, J. Hicks, G.P. Knowles, A.L. Chaffee, D.R. Turner, S.R. Batten. *Inorg. Chem.*, 55, 6692 (2016). (f) J. Ratilainen, K. Airola, R. Fröhlich, M. Nieger, K. Rissanen. *Polyhedron*, 18, 2265 (1999).
[31] H.K. Hall. Jr. *J. Am. Chem. Soc.*, 79, 5441 (1957).
[32] S.V.F. Beddoe, R.F. Lonergan, M.B. Pitak, J.R. Price, S.J. Coles, J.A. Kitchen, T.D. Keene. *Dalton Trans.*, 48, 15553 (2019).
[33] (a) H. Li, H. Hiang, H. Sun. *Acta. Crystallogr. Sect. E: Crystallogr. Commun.,* 67, 1372 (2011). (b) P. Cortés, A.M. Atria, M.T. Garland, R. Baggio. *Acta Crystallogr. Sect. C.: Struct. Chem.*, 62, 311 (2006). (c) A. El-Toukhy, G.Z. Cai, G. Davies, T.R. Gilbert, K.D. Onan, M. Veidis. *J. Am. Chem. Soc.,* 106, 4596 (1984). (d) A.M. Atria, A. Vega, M. Contreras, J. Valenzuela, E. Spodine. *Inorg. Chem.,* 38, 5681 (1999). (e) S. Löw, J. Becker, C. Würtele, A. Miska, C. Kleeberg, U. Behrens, O. Walter, S. Schindler. *Chem. Eur. J.,* 19, 5342 (2013). (f) G.A. van Albada, M. Ghazzali, K. Al Farhan, J. Reedijk. *Inorg. Chem. Commun.,* 14, 1149 (2011). (g) A.S. Lyakhov, P.N. Gaponik, M.M. Gegtyarik, L.S. Ivashkevich. *Acta Crystallogr. Sect. C: Struct. Chem.,* 60, 399 (2004). (h) K. Skorda, T.C. Stamatatos, A.P. Vafiadis, A.T. Lithoxoidou, A. Terzis, S.P. Perlepes, J. Mrozinski, C.P. Raptopoulou, J.C. Plakatouras, E.G. Bakalbassis. *Inorg. Chim. Acta*, 358, 565 (2005). (i) S. Becker, U. Behrens, S. Schindler. *Eur. J. Inorg. Chem.*, 2437 (2015). (j) N.S. Gill, M. Sterns. *Inorg. Chem.*, 9, 1619 (1970). (k) G.A. Bowmaker, C. Di Nicola, F. Marchetti, C. Pettinari, B.W. Skelton, N. Somers, A.H. White. *Inorg. Chim. Acta,* 375, 31 (2011).
[34] A.W. Addison, T.N. Rao, J. Reedijk, J. van Rijn, G.C. Verschoor. *J. Chem. Soc., Dalton Trans.*, 1349 (1984). doi:10.1039/DT9840001349
[35] L. Yang, D.R. Powell, R.P. Houser. *Dalton Trans.*, 955 (2007). doi:10.1039/B617136B
[36] (a) S. Sailaja, M.V. Rajasekharan.*Inorg. Chem.*, 42, 5675 (2003). (b) R.P. Feazell, C.E. Carson, K.K. Klausmeyer. *Inorg. Chem.*, 45, 935 (2006). [16411733]